Supplemental Information

Supplemental Figures

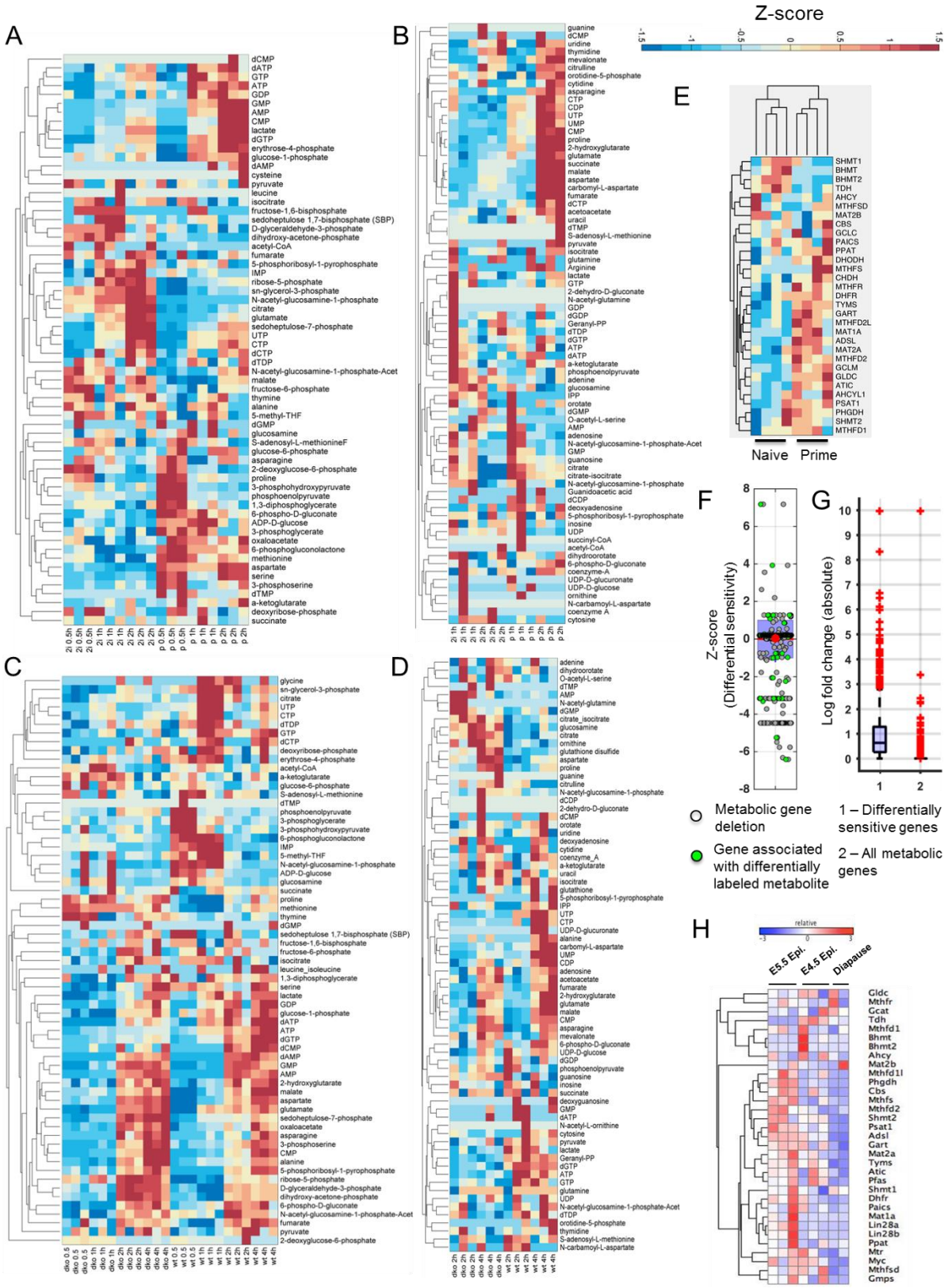
A
dCMP
dATP
GTP
ATP
GDP
GMP
AMP
CMP
lactate
dGTP
erythrose-4-phosphate
glucose-1-phosphate
dAMP
cysteine
pyruvate
leucine
isocitrate
fructose-1,6-bisphosphate
sedoheptulose 1,7-bisphosphate (SBP)
D-glyceraldehyde-3-phosphate
dihydroxy-acetone-phosphate
acetyl-CoA
fumarate
5-phosphoribosyl-1-pyrophosphate
IMP
ribose-5-phosphate
sn-glycerol-3-phosphate
N-acetyl-glucosamine-1-phosphate
citrate
glutamate
sedoheptulose-7-phosphate
UTP
CTP
dCTP
dTDP
N-acetyl-glucosamine-1-phosphate-Acet
malate
fructose-6-phosphate
thymine
alanine
5-methyl-THF
dGMP
glucosamine
S-adenosyl-L-methionineF
glucose-6-phosphate
asparagine
2-deoxyglucose-6-phosphate
proline
3-phosphohydroxypyruvate
phosphoenolpyruvate
1,3-diphosphoglycerate
6-phospho-D-gluconate
ADP-D-glucose
3-phosphoglycerate
oxaloacetate
6-phosphogluconolactone
methionine
aspartate
serine
3-phosphoserine
dTMP
a-ketoglutarate
deoxyribose-phosphate
succinate
2i 0.5h
2i 0.5h
2i 0.5h
2i 1h
2i 1h
2i 1h
2i 2h
2i 2h
2i 2h
p 0.5h
p 0.5h
p 0.5h
p 1h
p 1h
p 1h
p 2h
p 2h
p 2h
B
guanine
dCMP
uridine
thymidine
mevalonate
citrulline
orotidine-5-phosphate
cytidine
asparagine
CTP
CDP
UTP
UMP
CMP
proline
2-hydroxyglutarate
glutamate
succinate
malate
aspartate
carbomyl-L-aspartate
fumarate
dCTP
acetoacetate
uracil
dTMP
S-adenosyl-L-methionine
pyruvate
isocitrate
glutamine
Arginine
lactate
GTP
2-dehydro-D-gluconate
N-acetyl-glutamine
GDP
dGDP
Geranyl-PP
dTDP
dGTP
ATP
dATP
a-ketoglutarate
phosphoenolpyruvate
adenine
glucosamine
IPP
orotate
dGMP
O-acetyl-L-serine
AMP
adenosine
N-acetyl-glucosamine-1-phosphate-Acet
GMP
guanosine
citrate
citrate-isocitrate
N-acetyl-glucosamine-1-phosphate
Guanidoacetic acid
dCDP
deoxyadenosine
5-phosphoribosyl-1-pyrophosphate
inosine
UDP
succinyl-CoA
acetyl-CoA
dihydroorotate
6-phospho-D-gluconate
coenzyme-A
UDP-D-glucuronate
UDP-D-glucose
ornithine
N-carbamoyl-L-aspartate
coenzyme A
cytosine
2i 1h
2i 1h
2i 1h
2i 2h
2i 2h
2i 2h
p 1h
p 1h
p 1h
p 2h
p 2h
p 2h
Z-score
-1.5
-1
-0.5
0
0.5
1
1.5
E
SHMT1
BHMT
BHMT2
TDH
AHCY
MTHFSD
MAT2B
CBS
GCLC
PAICS
PPAT
DHODH
MTHFS
CHDH
MTHFR
DHFR
TYMS
GART
MTHFD2L
MAT1A
ADSL
MAT2A
MTHFD2
GCLM
GLDC
ATIC
AHCYL1
PSAT1
PHGDH
SHMT2
MTHFD1
Naive
Prime
C
glycine
sn-glycerol-3-phosphate
citrate
UTP
CTP
dTDP
GTP
dCTP
deoxyribose-phosphate
erythrose-4-phosphate
acetyl-CoA
a-ketoglutarate
glucose-6-phosphate
S-adenosyl-L-methionine
dTMP
phosphoenolpyruvate
3-phosphoglycerate
3-phosphohydroxypyruvate
6-phosphogluconolactone
IMP
5-methyl-THF
N-acetyl-glucosamine-1-phosphate
ADP-D-glucose
glucosamine
succinate
proline
methionine
thymine
dGMP
sedoheptulose 1,7-bisphosphate (SBP)
fructose-1,6-bisphosphate
fructose-6-phosphate
isocitrate
leucine_isoleucine
1,3-diphosphoglycerate
serine
lactate
GDP
glucose-1-phosphate
dATP
ATP
dGTP
dCMP
dAMP
GMP
AMP
2-hydroxyglutarate
malate
aspartate
glutamate
sedoheptulose-7-phosphate
oxaloacetate
asparagine
3-phosphoserine
CMP
alanine
5-phosphoribosyl-1-pyrophosphate
ribose-5-phosphate
D-glyceraldehyde-3-phosphate
dihydroxy-acetone-phosphate
6-phospho-D-gluconate
N-acetyl-glucosamine-1-phosphate-Acet
fumarate
pyruvate
2-deoxyglucose-6-phosphate
dko 0.5
dko 0.5
dko 0.5
dko 1h
dko 1h
dko 1h
dko 2h
dko 2h
dko 2h
dko 4h
dko 4h
dko 4h
wt 0.5
wt 0.5
wt 0.5
wt 1h
wt 1h
wt 1h
wt 2h
wt 2h
wt 2h
wt 4h
wt 4h
wt 4h
D
adenine
dihydroorotate
O-acetyl-L-serine
dTMP
AMP
N-acetyl-glutamine
dGMP
citrate_isocitrate
glucosamine
citrate
ornithine
glutathione disulfide
aspartate
proline
guanine
citrulline
N-acetyl-glucosamine-1-phosphate
dCDP
2-dehydro-D-gluconate
dCMP
orotate
uridine
deoxyadenosine
cytidine
coenzyme_A
a-ketoglutarate
uracil
isocitrate
glutathione
5-phosphoribosyl-1-pyrophosphate
IPP
UTP
CTP
UDP-D-glucuronate
alanine
carbomyl-L-aspartate
UMP
CDP
adenosine
acetoacetate
fumarate
2-hydroxyglutarate
glutamate
malate
CMP
asparagine
mevalonate
6-phospho-D-gluconate
UDP-D-glucose
dGDP
phosphoenolpyruvate
guanosine
inosine
succinate
deoxyguanosine
GMP
dATP
N-acetyl-L-ornithine
cytosine
pyruvate
lactate
Geranyl-PP
dGTP
ATP
GTP
glutamine
UDP
N-acetyl-glucosamine-1-phosphate-Acet
dTDP
orotidine-5-phosphate
thymidine
S-adenosyl-L-methionine
N-carbamoyl-L-aspartate
dko 2h
dko 2h
dko 2h
dko 4h
dko 4h
dko 4h
wt 2h
wt 2h
wt 2h
wt 4h
wt 4h
wt 4h
F
Z-score
(Differential sensitivity)
8
6
4
2
0
-2
-4
-6
-8
Metabolic gene deletion
Gene associated with differentially labeled metabolite
G
Log fold change (absolute)
10
9
8
7
6
5
4
3
2
1
0
1
2
1 – Differentially sensitive genes
2 – All metabolic genes
H
relative
-3
0
3
E5.5 Epi.
E4.5 Epi.
Diapause
Gldc
Mthfr
Gcat
Tdh
Mthfd1
Bhmt
Bhmt2
Ahcy
Mat2b
Mthfd1l
Phgdh
Cbs
Mthfs
Mthfd2
Shmt2
Psat1
Adsl
Gart
Mat2a
Tyms
Atic
Pfas
Shmt1
Dhfr
Paics
Mat1a
Lin28a
Lin28b
Ppat
Mtr
Myc
Mthfsd
Gmps

Figure S1: (Related to Figure 3 and 4). Transcriptomics and fluxomics data ([U-^{13}C]-glucose and [U-^{13}C]-glutamine tracing data) in naïve, primed, wild type and Lin28 knockout (surrogate of naïve state) cells. A. ^{13}C-glucose incorporation over time highlights the flux rewiring in naïve (2i) and primed (p) states. Numbers next to abbreviations indicate hours in naïve or primed media. Metabolites showing significant differences (p-value < 0.05) between naïve and primed states are shown in Figure 2. **B.** ^{13}C-glutamine incorporation over time in naïve and primed state cells. **C.** ^{13}C-glucose incorporation over time highlights the flux rewiring in knockout and wild type. Numbers next to abbreviations indicate hours in labeling media. Metabolites showing significant differences (p-value < 0.05) between the two phenotypes are shown in Figure 3. **D.** ^{13}C-glutamine incorporation over time in wildtype and Lin28 knockout cells. **E.** RNA expression of one-carbon metabolism and nucleotide metabolism genes in naïve versus primed PS cells. F. Comparison of model predictions of gene sensitivity and 13C labeling data. Genes that encode enzymes associated with differentially labeled metabolites (p-value < 0.05) from 13C tracing data are shown in green. Metabolites associated with differentially sensitive genes (z-score > 2 or < -2) were more likely to be differentially labeled between the two states (p-value = 0.005, hypergeometric test). **G.** Comparison of model predictions of gene sensitivity and transcriptomics data. mRNA transcripts associated with the genes predicted by the model to be differentially sensitive had significantly higher differentially expression than other metabolic genes (p-value = 0.003, t-test). The plot shows absolute log(fold change) values to account for significant upregulation and downregulation. H. RNA expression of one-carbon metabolism and nucleotide metabolism genes in mouse pre-implantation epiblast (E4.5 Epi.), post-implantation epiblast (E5.5 Epi.) and diapause epiblast cells.

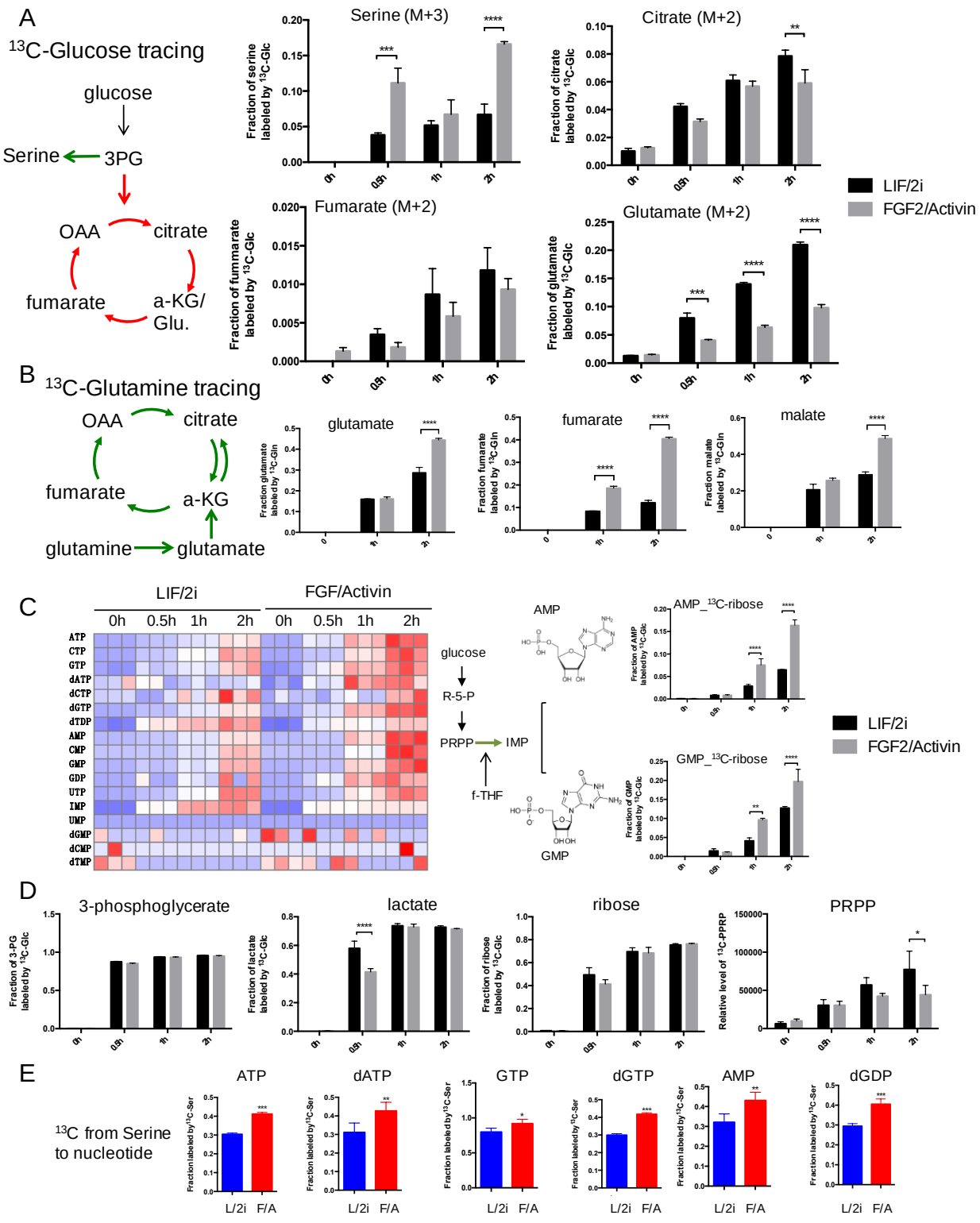
A
13C-Glucose tracing
glucose
Serine
3PG
OAA
citrate
fumarate
a-KG/
Glu.
Serine (M+3)
Citrate (M+2)
Fumarate (M+2)
Glutamate (M+2)
LIF/2i
FGF2/Activin
B
13C-Glutamine tracing
OAA
citrate
fumarate
a-KG
glutamine
glutamate
glutamate
fumarate
malate
C
LIF/2i
FGF/Activin
0h
0.5h
1h
2h
ATP
CTP
GTP
dATP
dCTP
dGTP
dTDP
AMP
CMP
GMP
GDP
UTP
IMP
UMP
dGMP
dCMP
dTMP
glucose
R-5-P
PRPP
IMP
f-THF
AMP
GMP
AMP_13C-ribose
GMP_13C-ribose
LIF/2i
FGF2/Activin
D
3-phosphoglycerate
lactate
ribose
PRPP
E
13C from Serine
to nucleotide
ATP
dATP
GTP
dGTP
AMP
dGDP
L/2i
F/A

Figure S2: (Related to Figure 3 and 4). [U-^{13}C]-glucose, [U-^{13}C]-glutamine and [U-^{13}C]-serine tracing in naïve and primed cells. A. ^{13}C-glucose incorporation to serine and the TCA cycle metabolites (isotopomers). Red colored arrow implies increased levels in the naïve state while green color implies decreased levels in the naïve state **B.**^{13}C-glutamine incorporation into the TCA cycle metabolites (isotopomers). **C.**^{13}C-glucose incorporation to the ribose moiety of nucleotides. **D.** ^{13}C-glucose incorporation to 3-phosphoglycerate, lactate, ribose-5-phosphate (R5P) and 5-phosphoribosyl-1-pyrophosphate (PRPP). **E**.^{13}C-serine incorporation at 2 hours to the nucleobase moiety of nucleotides. (Black bar is LIF/2i naive state and gray bar is FGF2/Activin primed state).

Supplemental Experimental Procedures

Cell culture

Mouse ES cells V6.5 (Novus, NBP1-41162) and iPS cells (wildtype and Lin28 knockout (Zhang et al., 2016)) were cultured in LIF/2i naïve media: 1000 u/ml LIF (Genimi), 1 μM PD03259010 and 3 μM CHIR99021 (Stemgent) were supplemented to a 1:1 mix of DMEM/F12 (Life Technologies) and Neurobasal medium (Life Technologies) containing N2 and B27 supplements (Life Technologies, 1:100 dilutions), penicillin/streptromycin, 0.1 mM 2-mercaptoethanol, and 2 mM L-glutamine. For primed media, 10 ng/ml FGF2 (Life Technologies), 20 ng/ml Activin (Thermo Fisher Scientific, and 1% KSR were supplemented to the 1:1 DMEM/F12 and Neurobasal medium containing N2 and B27 media, instead of LIF/2i. For metabolomics and drug-treatment experiments, cells in naïve condition and cells converted in primed condition for three days were cultured in parallel. Methotrexate was from Sigma-Aldrich, and the MTHFD2 inhibitor MTH-1459 was developed by Raze Therapeutics.

Benchmarking with NCI 60 cancer cell lines

To test our approach, we performed gene deletion analysis of all the metabolic genes in each of the NCI60 cancer cell line network models. We identified gene-cell line sensitive associations in which a specific gene was predicted to be essential in a given cell line. We then compared the predictions with data from two siRNA screens and a genome-wide CRISPR-Cas9 screen. Each study included a different subset of genes and cell lines, and used different statistical approaches to quantify sensitivity of gene knockouts. Hence these studies provide independent validation of our approach. Flux through ATP synthesis was used as the objective for assessing viability for comparison with Aguirre et al. 2016 (Aguirre et al., 2016) and Cheung et al. 2011 (Cheung et al., 2011) data, since the ATARIS score correlates with the change in ATP levels over time (Shao et al., 2013). In addition, flux through biomass synthesis was used as an additional metric for comparison with the GARP score from Koh et al (Koh et al., 2012), which tracks change in cell growth over time after shRNA treatment. These results are on par with the best performing method using gene expression data in these lines as measured by the KS-test (Pacheco et al., 2015). Gene knockouts with growth rates less than 95% of the wildtype growth rate were considered essential. Predictions were significant at both the 95% and 99% thresholds, which are commonly used by most genome-scale modeling studies (Folger et al., 2011; Pacheco et al., 2015). Decreasing the threshold to lower values (50%) to identify genes that strongly impacted growth or ATP flux in all cell lines further increased the consistency with CRISPR and siRNA screens (p-value = 1 x 10^{-5} for CRISPR and p-value = 1 x 10^{-17} for siRNA data).

Impact of alpha and beta vectors in the optimization problem

To account for noise in experimental data, positive vectors, alpha and beta, are introduced in the optimization problem to represent deviation from the measured experimental data.

$$\mathbf{S}.\vec{v} + \overrightarrow{alpha} - \overrightarrow{beta} = \overrightarrow{epsilon}$$

$$\textbf{Minimize } (\overrightarrow{alpha} + \overrightarrow{beta})$$

Removing these vectors or setting them to be zero implies that the model is directly fitted with the metabolomics data without allowing for "mismatches" between model predictions and experimental observations. This would lead to an infeasible solution as not all metabolomics measurements are simultaneously consistent with the network topology due to the various sources of noise (outlined earlier) in the metabolomic measurements. Conceptually, this optimization problem finds the best-fit state by minimizing the total deviation from experimental measurement. Minimizing the absolute value of a variable – in this case, the deviation from experimental measurement – is challenging to solve using standard linear optimization. The common way to solve this is by reformulating the absolute value into two linear expressions that represent the positive and negative component of that original function (Stephen Boyd and Lieven Vandenberghe and Cambridge University Press), as done here using alpha and beta vectors.

Approach pseudo-code

The pseudo-code below describes the sequence of steps in integrating metabolomics data with genome-scale models:

1. *Input: Metabolic network model, time-course metabolomics data*
2. *Calculate Flux activity coefficient (epsilon):*
    a. *epsilon = rate of change of metabolite per hour*
    b. *normalize epsilon using maximal value so that it is between -1 and 1 but relative magnitude and direction of change of metabolites is maintained*
3. *For each dynamic metabolite*

{

    a. *set the flux activity coefficient – R.H.S of the equation ($S.\vec{v}$ = b)*
    b. *create two pseudo-reactions ($\overrightarrow{alpha}$, $\overrightarrow{beta}$) that have positive flux; they account for positive and negative deviations respectively from the flux activity coefficient ($S.\vec{v}$ + $\overrightarrow{alpha}$ - $\overrightarrow{beta}$ = epsilon)*

}

4. *Once the metabolomics constraints are imposed, a single linear optimization problem is solved that minimizes the value of the pseudo-reactions (alpha, beta), thereby identifying the closest fit to the measured data, while simultaneously maximizing growth.*
5. *By default, equal weights (defined by kappa parameter) are provided for growth and metabolomics constraints. The kappa parameter (optional input) can be tuned to change the relative weights of growth over metabolomics constraints.*

Isotope tracing and metabolomics analysis

Isotope tracing and metabolomics studies were performed as described previously (Shyh-Chang et al., 2013; Yuan et al., 2012; Zhang et al., 2016). Briefly, 0.5-1x10^6 PS cells weaned from MEF feeders were cultured in naïve or primed media containing 25mM [U-^{13}C]-glucose or 2mM [U-^{13}C]-glutamine (Cambridge Isotope Laboratory) with indicated time. Cells were subsequently snap-frozen with cold 80% methanol on dry ice, followed by incubation at -80˚C from 15 min to overnight. Cells were scraped, collected and centrifuged at max speed for 15min at 4˚C, and the supernatant was evaporated with a speed vac at RT. Dried sample powder was resuspended with LC/MS grade water, and applied to a 5500 QTRAP Triple Quadrupole mass spectrometer (AB/SCIEX) coupled to a Prominence HPLC system (Shimadzu) using positive/negative polarity switching via selected reaction monitoring (SRM). Amide HILIC (Waters) chromatography was used for metabolite separation. MultiQuant 2.1 software (AB/SCIEX) was used to integrate peak areas from each SRM transition from both unlabeled and ^{13}C labeled metabolites.

The labeling intensity for a small number of metabolites were found to decrease at certain time points. This is due to the dilution of the heavy isotope 13C labeling by regular 12C over time, as there are other carbon sources in the media (Buescher et al., 2015). Further, the fluctuations in labeling patterns of some metabolites such as serine likely reflect exchange between intra- and extracellular pools and has been observed in 13C tracing data from both naïve cells and Lin28 knockout cells, and also in a prior study (Mullarky et al., 2016), suggesting that this is a real biochemical phenomenon.

Metabolites with missing values in over 25% of the measured conditions were discarded for modeling purposes. The intensity values for the final set of 103 metabolites that were consistently measured across naïve, primed, Δlin28 cells and across different time points are provided in supplementary Appendix. The total absolute levels of each

metabolite (sum of all labeled and unlabeled levels) was used for genome-scale metabolic modeling. No threshold was used for identifying dynamic metabolites; the estimated rate of change (dM/dt) from experiments were directly integrated into the model after normalization. For those metabolites that were not measured using metabolomics, we assumed that they are at steady state, which is the default assumption in FBA (dM/dt = 0).

For visualization of metabolomics data as heat-maps in Figures 2 and 3, the total levels of metabolite that was labeled from glucose or glutamine was used. The data was normalized to have zero mean and unit variance (z-transformation) prior to clustering and visualization. A value of +1 represents one standard deviation above the mean. This was done to visualize the entire data in a single scale and uniformly interpret change in metabolite levels.

Drug response and cell viability assay

Briefly, PS cells were weaned from MEFs, and 2500-5000 cells were seeded to one well of 96-well gelatin-coated plates. Cells in naïve or primed conditions were cultured in parallel for 3 days, with the last 2 days treated with drugs. On the day of measurement, cell viability was determined using the CellTiter-Glo-Luminescent Cell Viability Assay (Promega) according to the kit instruction.

Immunoblotting

Cells were lysed in RIPA buffer (Pierce) containing 1x protease inhibitor cocktail (Pierce). Protein was run on 15% SDS–PAGE, Abs included histone H3K4me3 antibody (Active Motif, 39160); histone H3K9me3 antibody (Active Motif, 39766) and histone H27K4me3 antibody (Active Motif, 39158). ECL Western blotting substrate (Pierce) was used for chemiluminescent detection.

Supplemental References

Boyd, S., and Vandenberghe, L., Convex Optimization. Cambridge University Press.

Buescher, J.M., Antoniewicz, M.R., Boros, L.G., Burgess, S.C., Brunengraber, H., Clish, C.B., DeBerardinis, R.J., Feron, O., Frezza, C., Ghesquiere, B., et al. (2015). A roadmap for interpreting 13C metabolite labeling patterns from cells. Curr. Opin. Biotechnol. *34*, 189–201.

Mullarky, E., Lucki, N.C., Beheshti Zavareh, R., Anglin, J.L., Gomes, A.P., Nicolay, B.N., Wong, J.C.Y., Christen, S., Takahashi, H., Singh, P.K., et al. (2016). Identification of a small molecule inhibitor of 3-phosphoglycerate dehydrogenase to target serine biosynthesis in cancers. Proc. Natl. Acad. Sci. *113*, 1778–1783.

Pacheco, M.P., John, E., Kaoma, T., Heinäniemi, M., Nicot, N., Vallar, L., Bueb, J.-L., Sinkkonen, L., Sauter, T., Gluckman, P., et al. (2015). Integrated metabolic modelling reveals cell-type specific epigenetic control points of the macrophage metabolic network. BMC Genomics *16*, 809.

Shao, D.D., Tsherniak, A., Gopal, S., Weir, B.A., Tamayo, P., Stransky, N., Schumacher, S.E., Zack, T.I., Beroukhim, R., Garraway, L.A., et al. (2013). ATARiS: Computational quantification of gene suppression phenotypes from multisample RNAi screens. Genome Res. *23*, 665–678.

Yuan, M., Breitkopf, S.B., Yang, X., and Asara, J.M. (2012). A positive/negative ion switching, targeted mass spectrometry-based metabolomics platform for bodily fluids, cells, and fresh and fixed tissue. Nat. Protoc. *7*, 872–881.